Averaged indicators of secondary flow in repeated acoustic Doppler current profiler crossings of bends

R. L. Dinehart and J. R. Burau

U.S. Geological Survey, Sacramento, California, USA

Received 21 February 2005; revised 11 May 2005; accepted 27 May 2005; published 3 September 2005.

[1] Cross-stream velocity was measured in a large river bend at high spatial resolution over three separate survey episodes. A suite of methods for resolving cross-stream velocity distributions was tested on data collected using acoustic Doppler current profilers (ADCP) in the sand-bedded Sacramento River, California. The bend was surveyed with repeated ADCP crossings at eight cross sections during a rising limb of high discharge in February 2004 and twice on recession in March 2004. By translating and interpolating repeated ADCP crossings to planar grids, velocity ensembles at similar positions along irregular boat paths could be averaged. The averaging minimized turbulent fluctuations in streamwise velocities over 1 m/s, enabling the resolution of weaker cross-stream velocities ($\sim$15–30 cm/s). Secondary-flow influence on suspended sediment was inferred from a lateral region of acoustic backscatter intensity aligned with outward flow over the point bar. A near-bed decrease in backscatter intensity across the pool corresponded with inward cross-stream flow. These suspension indicators were used to orient averaged velocity grids for unambiguously defining the cross-stream velocity magnitudes. Additional field investigations could test whether the correlation between cross-stream velocity and backscatter intensity patterns results from helical recirculation of suspended sediment to the inside of the bend. These river measurements, consistent with classic and recent laboratory studies, show that ADCP surveys can provide refined views of secondary flow and sediment movement in large rivers.

Citation: Dinehart, R. L., and J. R. Burau (2005), Averaged indicators of secondary flow in repeated acoustic Doppler current profiler crossings of bends, *Water Resour. Res.*, *41*, W09405, doi:10.1029/2005WR004050.

1. Introduction

[2] Vectorial methods for averaging measured velocity fields were tested using cross-sectional data collected with an acoustic Doppler current profiler (ADCP) along river bends. Through spatial averaging, we hoped to measure cross-stream velocities at greater resolution than usually attained for deep rivers during high discharge. In standard approaches, mean flow directions are derived across open channels by combining a series of velocity vector measurements enduring longer than the dominant timescales of turbulence. Turbulent velocity fluctuations that persist for seconds to minutes are smoothed by extended measurement times at each position. The special case of velocity fields in a bend requires two or three vector components in time-averaged velocity profiles to be measured sequentially across sections [e.g., *Bathurst et al.*, 1977; *Rodriguez et al.*, 2004].

[3] With present instrument designs, a single crossing of a river by a vessel-mounted ADCP can sample velocity profiles with three-dimensional (3-D) vectors at hundreds of locations. Although ADCP sampling rates near 1 Hz increase lateral resolution of velocity distribution in a natural channel, the velocity profiles are sampled briefly and thereby incorporate macroscale turbulence. In addition, the turbulent cross-stream fluctuations in bends are influenced by the mean cross-stream velocity, which is about one fourth the mean streamwise velocity [*Nezu and Nakagawa*, 1993]. Knowing that velocity profiles have indeterminate means in single ADCP crossings, we obtained repeated crossings along linear routes to allow grid-based averaging.

[4] From the central limit theorem, the standard deviation of many averaged crossings is expected to approach the population standard deviation. Statistical tests used in this study confirmed that a spatial average of five or more crossings halved the standard deviation for zero mean components (Appendix A). Although reducing standard deviation depends on optimized instrument settings for channel conditions, limited cross-sectional averaging generated near-mean velocity measurements at high spatial resolution. This survey strategy was designed to study effects of secondary circulation on the distribution of juvenile salmon within bends of the lower Sacramento River.

[5] By using the ADCP, we also recorded acoustic backscatter intensity, which is an accepted indicator of sediment suspension [*Thorne and Hanes*, 2002; *Gartner*, 2004], although calibrations for suspended sediment concentration require extensive sediment sampling [e.g., *Land and Jones*, 2001; *Gartner and Cheng*, 2001]. The experimental procedures were tested at four bends in the lower Sacramento River during February–March 2004. The stud-

ied bends had a wide range of curvature radius, width, and discharge that provided ample data to validate our inferences, but for brevity we only present results from the sharpest bend. In this study, we extracted asymmetric patterns of backscatter intensity in bend surveys, apparently influenced by secondary flow, which have yet to be confirmed by sampling. Nonetheless, these results are presented to show that ADCPs can provide refined views of secondary flow and sediment movement in large rivers typically measured from boats. Therefore the river bends partly served as a proving ground for resolving cross-sectional velocity fields with ADCPs in any large river channel.

1.1. Experimental Background

[6] As Chinook salmon outmigrants navigate the lower Sacramento River on their way to San Francisco Bay, their migration paths may include a number of diversional sloughs and canals. Because some flow diversions are situated at river bends, we hypothesized that the outmigrants may be diverted into those channels in greater numbers than predicted by discharge alone, owing to secondary circulation. From previous field studies, we knew that cross-stream velocities could be resolved by averaging ADCP surveys [*Dinehart and Burau*, 2005], but their magnitude had not been measured with ADCPs in typical bends. Although the influence of secondary circulation on salmon is not discussed here, the approach to measuring cross-stream velocities with ADCPs in the lower Sacramento River is presented here in detail.

[7] A reliable domain for finding cross-stream velocity is a sharp river bend. The centrifugal and pressure forces in bends induce a secondary flow that lies in a plane perpendicular to the primary flow direction. Secondary flow in bends is well known and has long been investigated in rivers and laboratory flumes [e.g., *Prandtl*, 1952; *Rozovskii*, 1957] and more recently modeled with depth-scale predictions of flow properties, sediment transport, or bed topography [e.g., *Odgaard*, 1981; *Bridge and Jarvis*, 1982; *Dietrich and Smith*, 1983, 1984; *Nelson and Smith*, 1989; *Kawai and Julien*, 1996; *Julien and Anthony*, 2002; *Blanckaert and Graf*, 2004]. The hydrodynamics of meander bends are outside the scope of this paper, but the field methods shown here may contribute to future investigations of bends in large rivers.

[8] By averaging several crossings within each cross section of a bend, we approximated time-mean velocity fields and inferred suspended sediment distributions seldom observed in large rivers. To validate these observations, this paper describes the ADCP survey procedures, and then shows the processing of ADCP data in two stages: (1) processing velocity ensembles and backscatter intensity from single ADCP crossings, and (2) using cross-sectional averages of backscatter intensity fields to reorient averaged velocity grids. The results at each data-processing stage provide insights into the velocity and sediment suspension fields, first at a macroturbulent scale, and then for mean flow field properties.

1.2. Present Uses of ADCPs in Open-Channel Flow

[9] The use of ADCPs for discharge measurement has been described and reviewed widely [*Gordon*, 1989, 1996; *Simpson and Oltmann*, 1993; *Simpson*, 2001; *Shields et al.*, 2003]. Commercial ADCPs are now routinely used in hydrographic offices for discharge measurements, yet this same device can also be used to study 3-D flow fields [*Dinehart and Burau*, 2005]. Routine ADCP operations [*U.S. Geological Survey*, 2001] need only be slightly modified to obtain detailed 3-D flow fields in river bends. The procedural modifications include the use of multiple linear crossings at multiple cross sections, internal ADCP averaging of velocity profile measurements, and postprocessing of ADCP measurements as described later.

[10] While recording velocity, an ADCP also records intensity of acoustic backscatter from the ensonified flow volume. After correction for radial spreading and fluid absorption, backscatter intensity varies primarily with the volume concentration of particles suspended in the flow [*Gordon*, 1996]. Acoustic backscatter provides first-order estimates of sediment concentration if the ADCP output is normalized and then calibrated to sediment concentration samples [*Deines*, 1999; *Holdaway et al.*, 1999; *Gartner*, 2002, 2004] or to other calibrated instruments [*Hill et al.*, 2003]. For instance, commercial programs such as Sediview [*Land and Jones*, 2001] calibrate sediment concentration samples to backscatter intensity recorded from ADCPs manufactured by RD Instruments. The ADCP surveys of this study did not include physical sampling of sediment concentration, so cross-sectional distributions of backscatter intensity, not sediment concentration, are presented. Because ADCPs are widely deployed for river discharge measurements in fresh water, the abundant backscatter data compels us to examine their utility as a sediment suspension tracer in secondary flow.

[11] Depth-scale, spanwise clouds of backscatter intensity are common in single ADCP crossings of the lower Sacramento River. The backscatter intensity clouds were interpreted as indicators of turbulent sediment suspension (“suspension indicators”), in keeping with current understanding of sediment transport in turbulent boundary layers. Correlations in open-channel flows between coherent structures and pulses of sediment concentration indicate the presence of sediment-suspending turbulent structures [e.g., *Sumer and Deigaard*, 1981; *Rood and Hickin*, 1989; *Grass et al.*, 1991; *Kostaschuk and Church*, 1993]. In rivers, coherent structures may occupy the flow depth and extend a distance of several depths along the streamwise direction [*Ashworth et al.*, 1996]. Numerous field studies have shown the association of depth-scale turbulent fluctuations and sediment suspension using non-ADCP devices in alluvial channels [*Lapointe*, 1992; *Kostaschuk and Church*, 1993; *Dinehart*, 1999; *Kostaschuk*, 2000]. At the time of this study, the acquisition of ADCP data had recently attained sufficient sampling density to capture indicators of turbulent sediment suspension in rivers.

[12] Processing and analysis methods are emphasized in this article because standard ADCP surveys do not resolve the velocity field by averaging repeated crossings over accurate bathymetry. Instead, velocity fields measured by standard methods are affected by errors from vector outliers and from biases in geographic positions, bathymetry, or vertical velocity. Backscatter intensity data, if examined in standard surveys, are not refined sufficiently for indicating

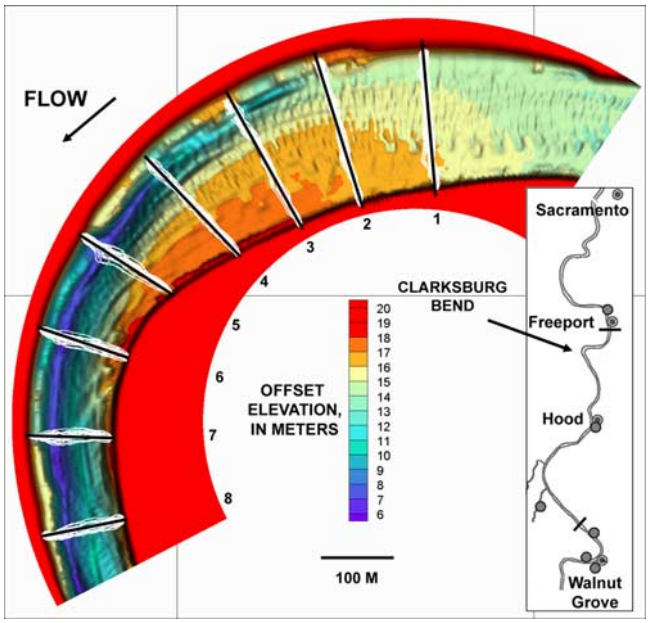

Figure 1. Map of sharp bend that was surveyed near Clarksburg in the lower Sacramento River, California, during study period, 9 February to 30 March 2004. Bathymetric points (in white) from six ADCP crossings are plotted at each of eight sections, 14 March 2004. The underlying contour map was interpolated from a reconnaissance survey made before the cross-sectional surveys. Flow directions are southward (downward on page).

sediment suspension. After correcting several elements of ADCP surveys with the described methods, the weaker cross-stream velocities can be resolved in secondary flow.

2. Survey Procedures

[13] The Sacramento River Delta has evolved through deposition of sandy sediment transported from the watersheds of the Central Valley in California. Discharge in the lower Sacramento River is influenced by oceanic tides that propagate into San Francisco Bay and through Suisun Bay, east of the city of San Francisco. For this study, the bend in the Sacramento River near Clarksburg (Figure 1) was surveyed following a discharge rise from winter rainstorms, when steadier flow conditions prevailed and tidal effects were minimal (Figure 2).

[14] A reconnaissance survey for coarse bathymetry in the Clarksburg bend was made by ADCP on 9 February 2004, prior to increased discharge during 16–19 February. Dune bed forms were measured along a depositional point bar which occupied the inner portion of most cross sections. The outside margin of the bend was approximated to a single circle, with eight cross sections spaced every 15 degrees from the entrance. Depths ranged from 7 to 10 m at the bend entrance to more than 15 m in the pool at the outside of the bend. The channel deepened progressively along the pool while decreasing its top width from 220 to 130 m. The mean radius of curvature was 0.56 km, with a ratio of 0.39 for the entrance width to radius. In the Sacramento River at Freeport, about 3 km upstream from the Clarksburg bend, sandy bed material has been sampled periodically with mean grain diameters ranging from 0.3 to 0.5 mm (U.S. Geological Survey, Water resources data—California, U.S. Geological Survey Water Data Reports CA55-2 through CA-99-2).

[15] The ADCP surveys were conceived to test methods of resolving cross-stream velocity in a natural channel. Therefore physical samplings of sediment transport were not made, because ADCP methodology to measure cross-stream velocity, not geomorphology, was the main interest of the study. Personnel on the river were asked only to obtain repeated crossings of bends at designated cross sections.

[16] The measured velocity u in a turbulent flow is typically separated into a time mean U and a turbulent fluctuation u'. Because u' tends to be small, the mean vector components of U dominate the velocity field in an ADCP crossing defined by several hundred ensembles. For this reason, we optimized ADCP settings to measure velocity at close lateral distances. Spatial averaging would then differentiate the mean cross-stream components of U along the section from the cross-stream turbulent fluctuations u'. Spatial averaging also partly overcomes a random error in ADCP data arising from the "homogeneity assumption," which is described here.

[17] The Doppler principle is applied by the ADCP to measure water velocity under a simplifying "homogeneity assumption" of parallel streamlines in open-channel flow. The difference between a transmitted sound frequency f and a received sound frequency f' is a function of the velocity in water of suspended particles that scatter transmitted sound. For a moving transmitter, water velocity u is calculated as

$$u = c - \frac{f(c - v)}{f'} \tag{1}$$

where c is the speed of sound in water, and v is velocity of the transmitter. In measuring water velocity, four transducers on the device transmit sound in narrow beams through the water column. The beams are aimed downward at 20 degrees from the device's vertical axis, in an orthogonal arrangement. Software for the ADCP measures radial velocities along the four acoustic beams. A velocity magnitude and bearing are calculated from the angles and radial velocities according to the "homogeneity assumption" of parallel streamlines. Deviations from this assump-

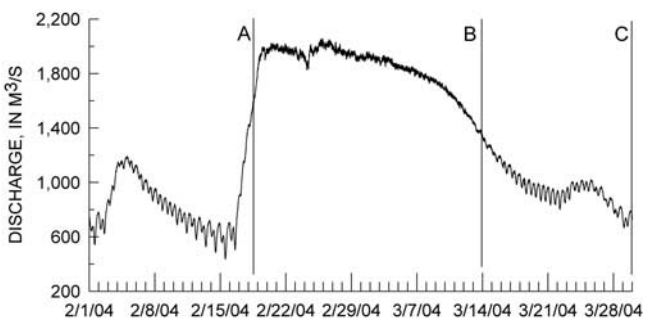

Figure 2. Discharge hydrograph for Sacramento River at Freeport, February–March 2004. Vertical lines indicate the time of ADCP surveys A–C at Clarksburg bend. Details of surveys are listed in Table 1.

tion are negligible in coherent water masses with minimal lateral and vertical shear, such as are typically found in marine environments. However, when open-channel flows include depth-scale turbulence at high intensities, streamlines will diverge below the ADCP in violation of the homogeneity assumption, reducing resolution of the measured velocity field [*Gordon*, 1996, p. 14; *Nystrom et al.*, 2002]. ADCP users are given only limited ability to detect distortion of measured velocity profiles in flow fields that are significantly nonhomogeneous.

[18] Conventional procedures for ADCP data acquisition are given by *Simpson* [2001], while an overview of modified procedures is given here. The ADCPs used in the Sacramento River were Workhorse models (RD Instruments, Inc.) operating at 1200 kHz. When an ADCP is mounted on a boat, beams 1 and 2 transmit outward, perpendicular to the keel line, and beams 3 and 4 transmit fore and aft. For each sound transmission (''ping''), a vertical set of velocity magnitudes and bearings is measured through the water column. The set of velocities recorded at each geographic position is a ''velocity ensemble,'' which can be derived from one ping or the average of multiple pings. The horizontal slice of water represented by a single velocity measurement in the water column is a ''bin.'' The sampling time per ensemble depends on configuration settings such as the number of pings per ensemble, the number and height of bins, the data communication rate, and the bottom-tracking settings. Recorded velocity ensembles contain only vector data measured from nearly 1 m below the water surface to more than 1 m above the bed.

[19] Three ensemble pings were averaged before transmitting each velocity ensemble. The recording of multiple-ping ensembles lowers the standard deviation of transmitted velocity ensembles by a factor proportional to the number of pings [*Gordon*, 1996]. Although velocities in multiple-ping ensembles are subject to errors generated by velocity ambiguity as defined by *Gordon* [1996], such errors are rare and recognizable. Recording multiple-ping ensembles with reduced standard deviation is an essential stage in identifying the weaker cross-stream velocities. The standard deviation and sampling time were further reduced by increasing the height of bins to 0.4 m. The sampling time per velocity ensemble consequently ranged from 1.0 to 1.3 seconds. With typical boat speeds of 1 to 2 m/s, the number of velocity ensembles per crossing ranged from 200 to more than 300. Up to six ADCP crossings per hour were obtained for subsequent averaging.

[20] The lateral velocity of the ADCP is determined by acoustic reference to the bottom (''bottom tracking'') or by GPS navigation. A differential GPS receiver (Trimble Ag132) was integrated with the ADCP to obtain horizontal geographic coordinates at 5 Hz. Each cross section of a bend was drawn on a digital map, which the boat pilot followed closely using GPS navigation. Any GPS positional errors caused by interference near river banks were corrected using bottom-tracking segments bracketed by reliable GPS positions [*Dinehart and Burau*, 2005]. The orientation of the ADCP is determined in most deployments by pitch and roll sensors and a built-in compass. The lateral ADCP velocity and orientation together specify the ADCP's velocity vector v in equation (1). Water-surface elevation was referenced to river stage as recorded at nearby gauging stations. All velocity ensembles were then referenced to vertical geographic datum through the offset between the transducer face and the water surface elevation.

[21] The ADCP-operating software WinRiver (RD Instruments, Inc.) was configured identically for data acquisition in all bend surveys. Three ADCP surveys (A-C) in the Clarksburg bend are summarized in Table 1. For ADCP surveys A and B, GPS was chosen over bottom tracking as the reference for ADCP velocity, due to bed movement inducing errors in bottom tracking that could affect v in equation (1). Water velocity was referenced to bottom tracking for survey C because bottom track effects on boat speed were minimal over the stable bed at lower stream velocity, as confirmed by comparisons with GPS positioning. The bottom-tracking reference yielded uniform vector distributions in velocity ensembles at cross sections, and avoided the random effects on boat speed of poor GPS reception near river banks.

3. Processing ADCP Data

[22] Data from ADCP crossings were processed beyond the internal filtering applied by WinRiver in computing discharge measurements. A series of custom algorithms were written and applied, including (1) velocity conversion and outlier filtering, (2) extraction of bed elevation from bathymetric grids below velocity ensembles, (3) near-bed extrapolation of velocity profiles, (4) mean offset application to vertical velocity, (5) near-point kriging interpolation of backscatter intensity, and (6) section straightening and averaging. Although the algorithms were designed for routine use, a few days of surveys required several weeks of processing and analysis. *Shields et al.* [2003] concluded that the study of river reaches with ADCPs is hampered by the lack of custom software for data analysis. We concur, noting that the present study used custom software designed for batch processing of ADCP measurements with data extraction, correction, visualization, and hydrodynamic analysis [*Dinehart*, 2003; *Dinehart and Burau*, 2005]. These programs converted ADCP data by the widely available Microsoft Excel with Visual Basic for Applications, and exported them for 3-D plotting and vector analysis in software by Tecplot (Tecplot, Inc.).

3.1. Processing of ADCP Velocity Ensembles

[23] During acquisition, ADCP velocity components are recorded as magnitude and bearing for horizontal velocity, and a signed magnitude for vertical velocity. After conversion, velocity vector components u and v are referred to two lateral directions (north and west positive) and the component w to a vertical direction (up positive). Until they are reoriented by trigonometric rotation, u and v do not refer to streamwise or cross-stream components.

[24] After data export from WinRiver, the ADCP velocity ensembles were imported and processed by a series of editing and filtering routines designed with Visual Basic for Applications [*Dinehart*, 2003], using several algorithm passes. One pass removed velocity vector components at the bottom of each ensemble that showed extreme outliers usually generated by velocity ambiguity. Velocity data were then numerically smoothed in two steps. Vector components

Table 1. Summary of ADCP Surveys in Sacramento River at the Clarksburg Bend, February–March, 2004

ADCP Survey	Date	Change in Stage, m	Mean Discharge, m^3/s	Mean Velocity at Sections, m/s	Number of ADCP Crossings
A	19 Feb 2004	0.10	1,580	1.10	4
B	14 Mar 2004	0.03	1,340	0.95	6
C	30 Mar 2004	0.10	679	0.58	6

exceeding the ensemble mean by 2.5σ (standard deviation) were first replaced directly by an average of nearest neighbors, to avoid distorting profiles in subsequent smoothing. This operation was followed by an optional, three-point average applied to all interior components of velocity ensembles, using the formula

$$u_b = 0.25u_{b-1} + 0.5u_b + 0.25u_{b+1} \quad (2)$$

where u_b signifies a vector component u, v, or w at an interior bin b. Although velocity magnitude profiles and vertically averaged velocities were little affected by three-point averaging [*Dinehart and Burau*, 2005], the 3-D vector displays were clarified by suppressing vector deviations between bins.

3.2. Velocity Profile Extrapolation to Bathymetry

[25] Reflection of transmitted ADCP signals from the channel bottom causes interference by acoustic side lobes and increases the uncertainty of near-bed velocities [*Simpson*, 2001]. To avoid contaminated data from sidelobe interference, velocity measurements within about $0.06d$ (depth) of the bed are discarded by WinRiver. In the surveyed bend, only velocities measured at least 1 to 1.5 m above the bed were retained. Velocity ensembles were extrapolated downward into the unmeasured velocity region by a replicable method. The resulting velocity profiles enabled grid-based calculation of discharge through surveyed channels. The unmeasured velocity region also contained backscatter intensity data which were then plotted at bins of the extrapolated velocity profiles.

[26] The ADCP velocity ensembles measured from a moving boat are not time-averaged, and seldom follow smooth distributions with height. Instead, ensembles exhibit turbulent fluctuations within the vertical profile, often with increased velocity in the bottom bins. Rather than fit near-bed profiles to turbulent structures, each velocity ensemble was extrapolated from the lowest valid velocity to zero velocity at the bed. The unmeasured region occupied at least the bottom 10% of depth, which is part of the inner region of a turbulent boundary layer. To estimate inner region velocity vectors, a law-of-the-wall logarithmic profile was applied:

$$\overline{u} = 5.75u_* \log\left(\frac{30y}{k_s}\right) \quad (3)$$

where $\overline{u}$ is the mean velocity at a distance y above the bed, and k_s is a roughness coefficient. Each unmeasured velocity vector $\mathbf{u} = u, v, w$ was computed at the near-bed bin elevations y using a form of equation (3) containing the shear velocity u_* as part of the term B, with u as an example,

$$u = B\log(Ay)$$

where

$$A = \frac{30}{k_s},$$

$$B = \frac{u_d}{\log(Ay_d)}$$

and the subscript d in the term B denotes the bin of the deepest valid velocity u_d at bin elevation y_d. The adjustable coefficient for roughness height, k_s, was approximated from ADCP discharge measurements and water surface slope between gauging stations. Using bin heights of 0.4 m, three or four velocities were calculated from equation (3) for the unmeasured region below each velocity ensemble.

[27] The set of ADCP crossings at each section acquired sufficient bed elevation data to map cross-sectional topography (Figure 1). Bed elevations were first calculated at each of four beam contacts for a set of crossings [*Dinehart and Burau*, 2005]. Bed elevation data were then interpolated into bathymetric grids as cross-sectional strips, with topography resolved to better than 1 m horizontally and 10 cm vertically. The bed elevation beneath each velocity ensemble was extracted from this bathymetric grid. This procedure reduced the typical error obtained by averaging four beam depths around each ensemble. The extracted bed elevation was then used with equation (3) for near-bed velocity extrapolation. The cross-sectional topography later defined the lower boundary for cross-sectional grids of ADCP data.

3.3. Negative Bias in Vertical Velocity

[28] Two types of instrument bias in ADCP vertical velocity were detected by averaging across velocity ensembles in single crossings: (1) a negative bias zone of vertical velocity extending 2 m below boat-mounted ADCPs and (2) an undiagnosed offset of the interior vertical velocity measurements from a zero mean. The first type of bias in vertical velocity was a negative offset around −2 to −4 cm/s. Examples of the negative bias zone were calculated from midchannel velocity ensembles in the Clarksburg bend and in a straight reach near Walnut Grove (Figure 3). In streamwise velocities above 100 cm/s, negative biases in vertical velocity exceeded −4 cm/s (Figures 3a and 3c). At lower streamwise velocities, negative bias in cross-sectional averages was less than −2 cm/s (Figures 3b and 3d).

[29] The negative bias zone appears to result from flow divergence past the survey boat. The difference in lateral velocity measured by two pairs of beams is assigned to vertical velocity by the WinRiver vector calculation algorithm (R. Marsden, RD Instruments, personal communication, 2004). The second type of bias in vertical velocity was found at most sections below the negative bias zone, with an offset about −2 cm/s from mean zero.

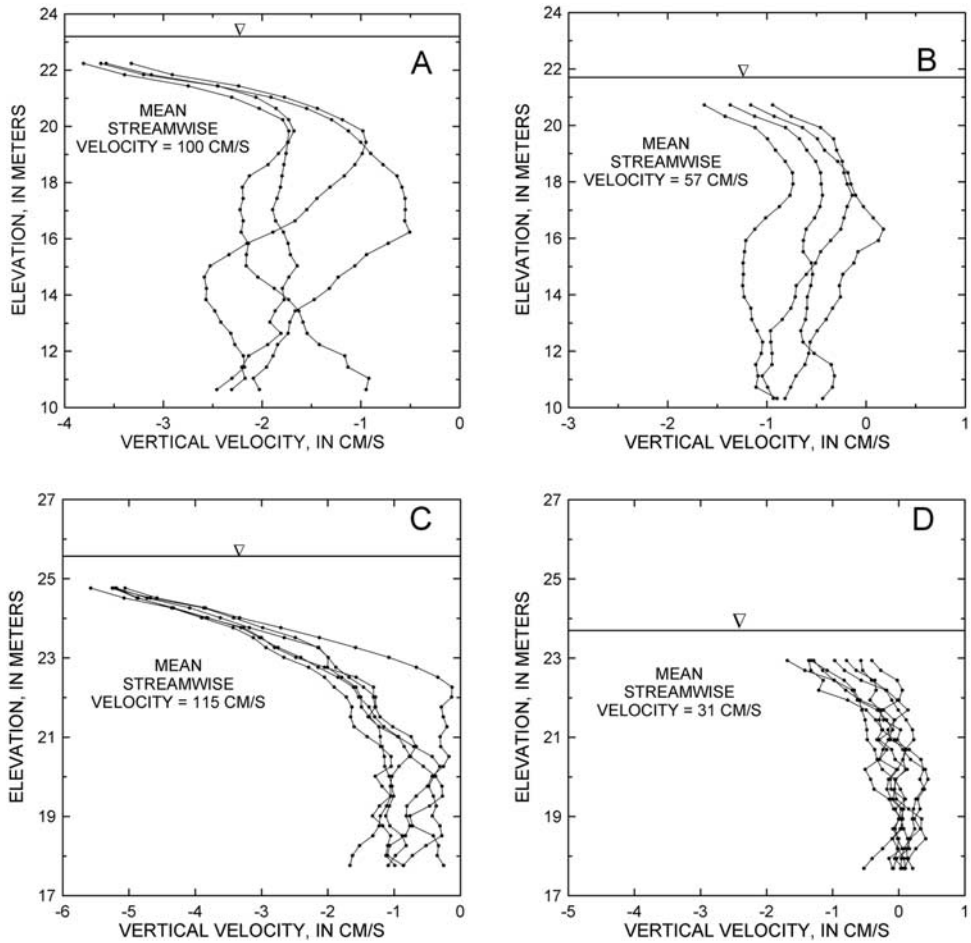

Figure 3. (top) Vertical velocity profiles of Sacramento River at Clarksburg bend showing zone of negative bias within 2 m of water surface at (a) high and (b) recessional discharge. Each profile is an average from a single ADCP crossing. (bottom) Vertical velocity profiles of Sacramento River above Walnut Grove at (c) high and (d) low discharge. Each profile is an average from a single ADCP crossing.

This undiagnosed offset increased with greater streamwise velocity (Figure 3).

3.4. Processing Backscatter Intensity

[30] Backscatter intensity is measured as the acoustic energy (in dB) returned from scattering particles. The WinRiver software (version 10.06) calculated backscatter intensity with a near-field correction that was not satisfactory for our needs. Instead, relative backscatter intensity (BI) was calculated from recorded intensity counts with the standard relation,

$$\mathrm{BI} = \mathrm{EIS} \times [\mathrm{counts}] + 20 \log R + 20\alpha R \qquad (4)$$

where EIS (echo intensity scale) = $127.3/(T_e + 273)$, in dB/counts, T_e is electronics temperature recorded near the ADCP transducer, R is distance to the ensonified volume, in meters, and α is sound absorption coefficient.

[31] Except for R, the variable values were obtained directly from the ADCP text output and processed with equation (4) as published by the manufacturer in WinRiver (RD Instruments, Inc.). The backscatter intensities are relative because no compensation is calculated for transmitted power [*Gartner*, 2004], but the power input was constant during each ADCP survey, providing a consistent indicator of sediment suspension.

[32] The ADCP records backscatter intensity counts from bins along four beams that outline a tetrahedral volume (Figure 4a). In this study, backscatter intensities were not averaged at the same bin elevations, but were mapped to their true positions in each beam to increase spatial resolution in the water column. A set of linear regressions was calculated between a reference beam (beam 1) and the remaining beams to normalize backscatter intensity. When plotted in the surveyed channel, the normalized backscatter intensity formed a set of points within each beam along the crossing path (Figure 4b). At greater depth, the backscatter intensity points plotted more distantly from the vertical axis of positions in the crossing path. By crossing slowly with the boat's bow aligned in the river current ("crabbing"), backscatter intensity points in the port and starboard beams (1 and 2) were usually closer to the crossing path than those in the fore and aft beams (3 and 4).

[33] Backscatter intensity points were interpolated by selective kriging in Tecplot to bin positions of velocity

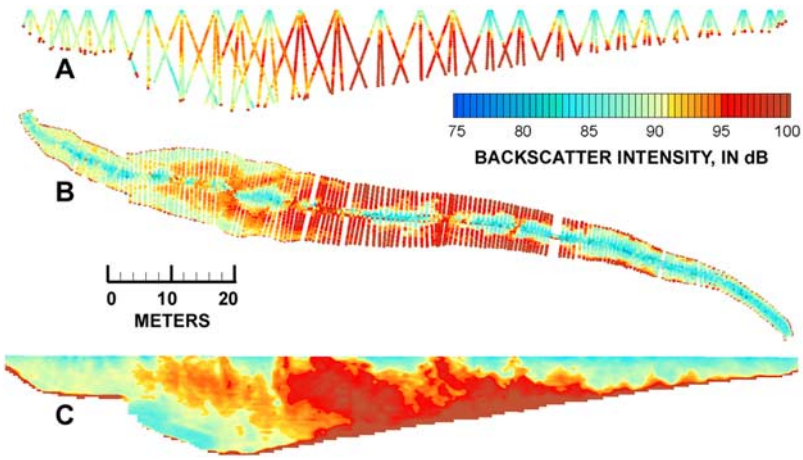

Figure 4. (a) Elevation and (b) plan views of backscatter intensities plotted at true positions of bins in four beam lines, Sacramento River at Clarksburg bend, single ADCP crossing. Every eighth ensemble is plotted in Figure 4a for clarity. Width of channel is about 70 m, and full depth is 15 m. In Figure 4b, flow is downward on the page. (c) Elevation view of kriged backscatter plane for same ADCP crossing. Both elevation views are upstream.

ensembles along the crossing path. Points measured in beams 1 and 2 were favored by kriging because of their spatial distribution. Six source points were chosen for each interpolation. The kriging range of source points was limited vertically around each target bin beneath the ADCP positions. As a result, the boundaries of backscatter intensity regions were sharpened by excluding laterally distant points (Figure 4c), with boundary gradients of 4 dB/m or more. The tradeoff was a loss of time synchrony as backscatter intensity points from several sequential ensembles were kriged to single ensemble positions. During survey crossings, the streamwise variation in structures appears to be more gradual than the lateral variation, so time synchrony is less critical to the interpolation accuracy.

3.5. Indicators of Turbulent Sediment Suspension

[34] Although single ensembles in ADCP data are processed with a bin-weighting function [*Gordon*, 1996], adjacent velocity ensembles are sampled independently during acquisition. Progressive variations in vectors across several velocity ensembles were common to single ADCP crossings. These variations along oblique patterns, extending over one third or more of the flow depth, indicated that coherent structures or "large scale vortical motions" [*Nezu and Nakagawa*, 1993] are probably recorded in rapid sampling during single ADCP crossings (Figure 5). Coherent structures cannot be identified directly in ADCP crossings because cross-sectional velocity profiles do not trace the evolution of the correlated velocity directions within the flow. The lateral distance between ADCP beams equals about $0.7h$, so smaller coherent structures may not be resolved by ADCPs. However, an ADCP sampling of deep flows at 1 Hz with a moderate crossing speed can acquire several velocity ensembles within a coherent structure, rendering it detectable in spanwise velocity displays.

[35] With backscatter intensity clouds resolved by kriging, the plots of ADCP crossings indicated local regions of turbulent sediment suspension more clearly (Figure 5). The expected relation of suspension indicators to the turbulent flow field follows from previous work in sand bed rivers. *Lapointe* [1992] acquired optical backscatter signals and streamwise/vertical velocity fluctuations in a sand-bedded

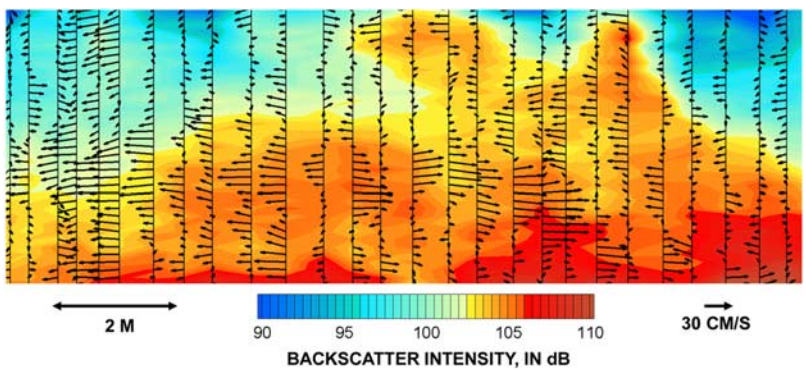

Figure 5. Central segment (10 m wide) of single ADCP crossing at straight reach in Sacramento River above Walnut Grove, showing cross-stream vectors with coherent directions across adjacent velocity ensembles. The lateral distance is exaggerated 2.5 times the vertical. Only the measured velocity region is shown. View is upstream; the crossing view is perpendicular to mean flow direction.

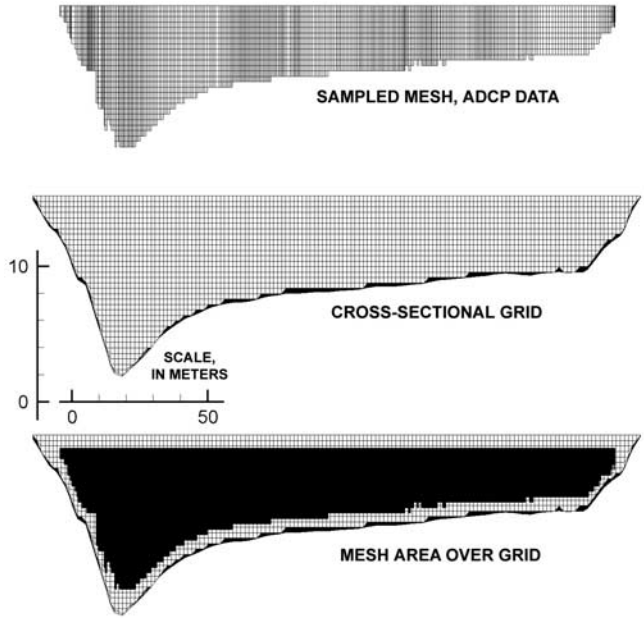

Figure 6. Example of an *i-j* ordered grid for interpolated velocity fields with extra *j* nodes in cross-sectional grid isolated to unmeasured region near bed. The sampled range of measured data is shown by the mesh area over the grid.

reach of the Fraser River. He analyzed characteristic increases in vertical velocity corresponding with increases in optical backscatter intensity. Strong, instantaneous upwelling of flow in velocity records, when accompanied by flow deceleration, was correlated with the highest intensities of optical backscatter. Correlated occurrences of upwelling and increased backscatter were termed ''burst-like sediment suspension events.'' After converting these events to sediment flux, *Lapointe* [1996] estimated that intense sediment flux events exceeded the mean flux by a factor of ten between 1 and 5% of the time. In ADCP crossings, the probability of encountering true sediment suspension events should be much lower than for detecting backscatter intensity clouds. Where near-bed regions of vertical velocities are closely associated with higher backscatter intensities, the ADCP may have recorded active suspension by coherent structures. However, the association of high backscatter regions with coherent structures is not exclusive in single ADCP crossings. For our purposes, the backscatter intensity clouds are considered localized, advecting suspended sediment at volume concentrations greater than their surroundings, regardless of any correlation with the velocity field.

3.6. Straightening ADCP Crossings

[36] A small boat crabbing slowly across a large river is unlikely to follow a straight line. The interaction between pilot steering, lateral shear, and river turbulence, can push the boat off a linear course. To derive a bend-crossing plane of velocity vectors from ADCP data, a procedure of ''section straightening'' was developed to translate velocity ensembles spatially to a straight line.

[37] A mean crossing line was fitted through multiple crossing paths at each section (Figure 1). Ensemble positions were translated to the crossing line by cosine rotation on a long radius. A distant point on the crossing line was set as (x_s, y_s) and the distance L from the point to each ensemble location (x_e, y_e) was calculated. The new position (x_t, y_t) on the crossing line was calculated using the known angle θ between the crossing line and the x axis:

$$\begin{aligned} x_t &= x_s + L\cos\theta \\ y_t &= y_s + L\sin\theta \end{aligned} \tag{5}$$

Although some velocity ensembles were translated by several meters, the distance of translation was usually less than 10% of the channel width. After translation, the velocity ensembles still retained their original vector components along the new alignment. In most cases, the streamwise flow direction was not perpendicular to the mean crossing line, so cross-sectional grids were reoriented after averaging of the straightened crossings.

3.7. Grid Interpolation and Averaging of Straightened Crossings

[38] The measured and unmeasured velocity regions in a typical bend crossing is shown on a cross-sectional grid in Figure 6. In Tecplot, a cross-sectional grid is a 2-D matrix of geographic coordinates ordered by cross-stream position *i* and vertical position *j*. Any number of velocity vectors and data values can be assigned to the grid coordinates. The grid area included the entire cross section beyond the unmeasured velocity regions. The base line for a grid was set as the mean crossing line, and matched the vertical elevation of the bed in cross-sectional bathymetry. Distances between lateral *i* nodes equaled the section width divided by a constant number of verticals. The number was chosen to yield cell widths of 1 m, about twice the distance between ensembles along crossing paths.

[39] Vertical *j* nodes at each *i* position were extended to the bed from the same crossing line at the water surface. Cell heights were given the bin height used during ADCP surveys (0.4 m). The number of vertical *j* nodes at each *i* position equaled the maximum depth in the cross section divided by cell height. To maintain constant cell heights over irregular bathymetry in a cross-sectional grid, extra *j* nodes were assigned elevations within 0.3 m of the bed (Figure 6). This configuration maintained equal vertical spacing of vector components in the measured range of velocity, and isolated the extra *j* nodes into the unmeasured region near the bed.

[40] The velocity ensembles in straightened ADCP crossings were interpolated over very small distances to *i-j* grids using an inverse distance algorithm in Tecplot. The algorithm interpolated each vector at a target node from six source vectors selected by an equipartite arrangement. This prevented the algorithm from selecting source vectors on only one side of the target node, or only source vectors within the same ensemble. Target vectors represented only the nearest ensembles of the source mesh. Velocities at the top row of the crossing mesh were interpolated upward through the target grid to the water surface.

[41] Each set of interpolated grids was averaged together to arrive at a final velocity grid. Two interpolated grids at the Clarksburg bend, section 6, are shown in Figure 7a, with the averaged velocity grid (unrotated) for the same section. The interpolation step was taken first because the ensembles of each ADCP crossing were variably spaced by irregular paths and boat speeds. If all ADCP crossings were

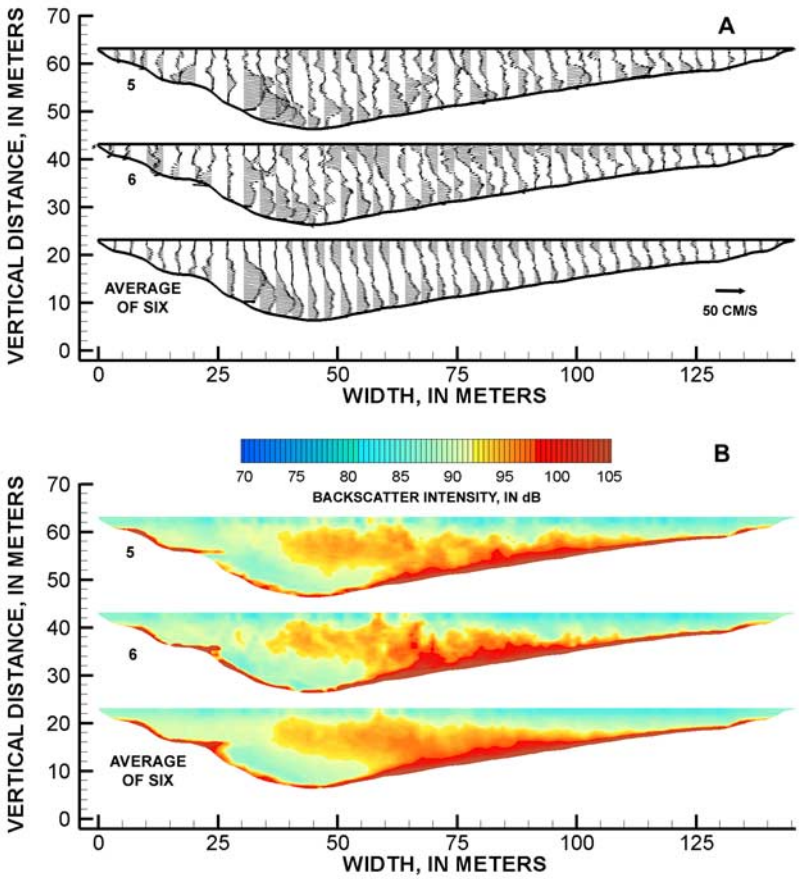

Figure 7. Cross-sectional plots for the Sacramento River at Clarksburg bend (section 6, 14 March 2004). (a) Interpolated, unadjusted velocity grids for single ADCP crossings (5 and 6) and the averaged velocity grid of all six crossings. Every third velocity ensemble is shown for clarity. (b) Interpolated backscatter planes for single ADCP crossings (5 and 6) and the average of all six crossings. Views are upstream.

interpolated directly to a single grid, turbulent structures in densely spaced crossings would be over weighted in the interpolation. Although the standard deviation of vector components was reduced by averaging ADCP crossings (Appendix A), the signature of some turbulent structures remained. Their vector components were usually far from the mean and were retained as spanwise deviations in averaged velocity grids. Grid averaging smoothed the turbulent fluctuations in vertical velocities, but retained time mean trends of downwelling at the pool and upward flow across the point bar.

[42] As noted, the four-beam backscatter intensities were interpolated to bin positions in each velocity ensemble along the crossing path. Those values were then translated unchanged with the target velocity ensembles to a mean crossing line. Thereafter, the interpolation and averaging of velocity grids were applied simultaneously to backscatter intensity values.

4. Techniques for Averaged Velocity Grids

[43] Techniques were developed to reorient averaged velocity grids for interpreting secondary circulation. An experimental procedure is shown for collectively rotating the vectors of an averaged velocity grid to match suspension indicators of the backscatter plane. This procedure estimated the orientation and consequent magnitude of cross-stream velocity vectors. The negative biases of vertical velocity affected the apparent secondary circulation, so offsets were derived from cross-sectional averages of vertical-velocity profiles.

4.1. Radial Fronts and Incurvatures in Bends

[44] The averaging of backscatter planes diffused the boundaries of suspension indicators while maintaining the time-averaged distribution and relative magnitude of cross-sectional backscatter intensity (Figure 7b). The averaged backscatter planes showed higher intensity in clouds over bars and near isolated bed forms, banks, or terraces. These suspension indicators are common in ADCP crossings of straight reaches [*Dinehart*, 2003].

[45] Uncommon suspension indicators were recorded at the bend sections in the presence of substantial cross-stream velocity. Width-scale structures called ''radial fronts'' repeatedly emerged in backscatter planes of the sharp bend (Figure 7b). Radial fronts are regions of increased backscatter intensity, usually elongated toward the outer bank and overhanging the bend pool, that have a swept appearance underneath and inward from the pool. The term ''radial front'' describes the probable influence of radial flow on the

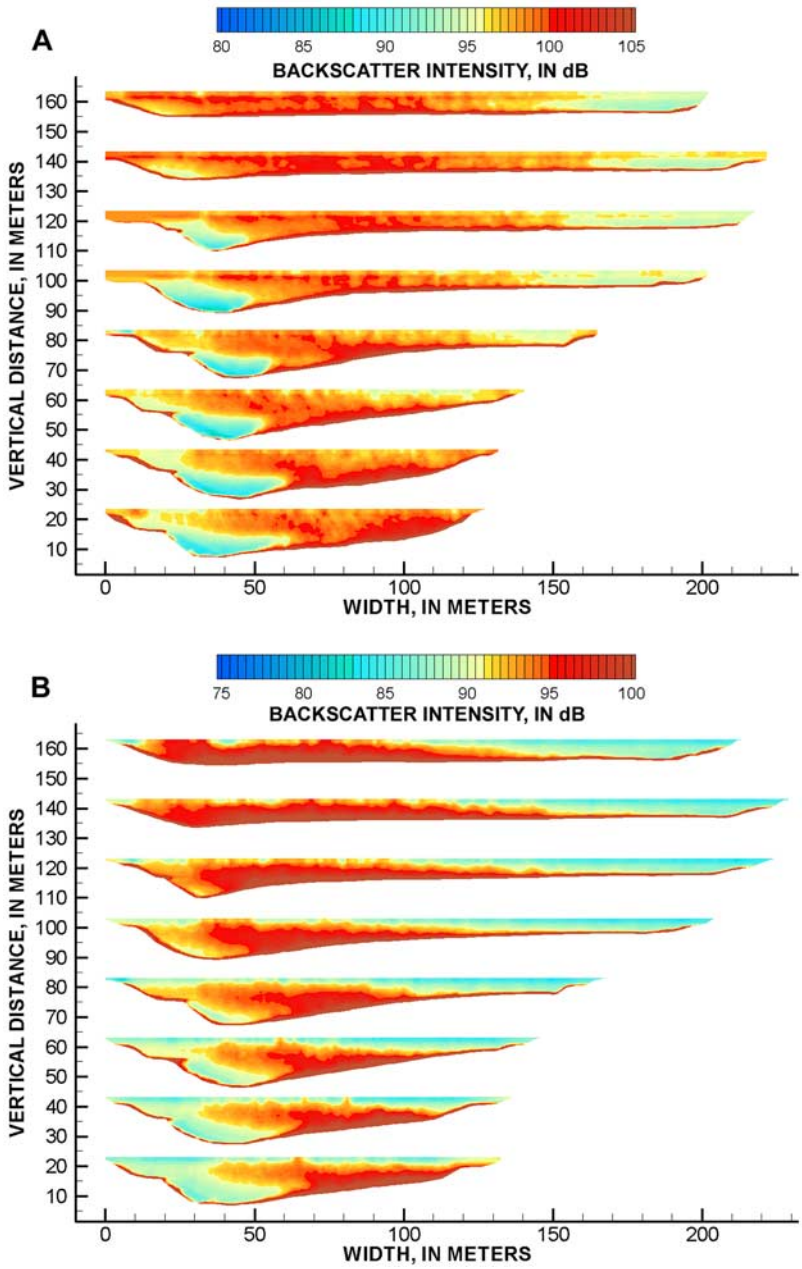

Figure 8. Cross-sectional plots of backscatter intensity for the Sacramento River at Clarksburg bend, surveys (a) A, (b) B, and (c) C, at all sections 1–8. The entrance section is at the top of each group, plotted in downstream order. Views are upstream.

lateral distribution of suspended sediment as inferred from backscatter intensity. This term is preferred to "plume," which indicates turbulent advection/diffusion from a central source without accounting for the circulation of secondary flow. Some radial fronts observed in the wider bends extended vertically through the entire water column, and extended outward with little overhang.

[46] All cross sections of averaged backscatter planes are plotted for surveys A to C at the Clarksburg bend (Figure 8). Progressing downstream, the centers of peak backscatter intensity in radial fronts migrated inward from the pool. In all surveys, the outer margins of radial fronts tended to coincide with convergence zones (regions near the outer bank where outward flow meets with poolward flow, having minimal cross-stream velocity and increased downwelling).

[47] The lower margins of radial fronts were bounded by a region of decreasing backscatter intensity across the pool that curved inward to the higher backscatter intensity over the bar. These "incurvatures" corresponded with inward vectors in the unadjusted cross-stream velocity field (Figure 7). Over the point bar, cross-stream vectors were nearly perpendicular to contour lines at the narrow incurvature boundary, suggesting inward migration of lower-concentration fluid. Above the incurvatures, backscatter intensity was inversely stratified, increasing vertically to a peak value in the middepth region where cross-stream

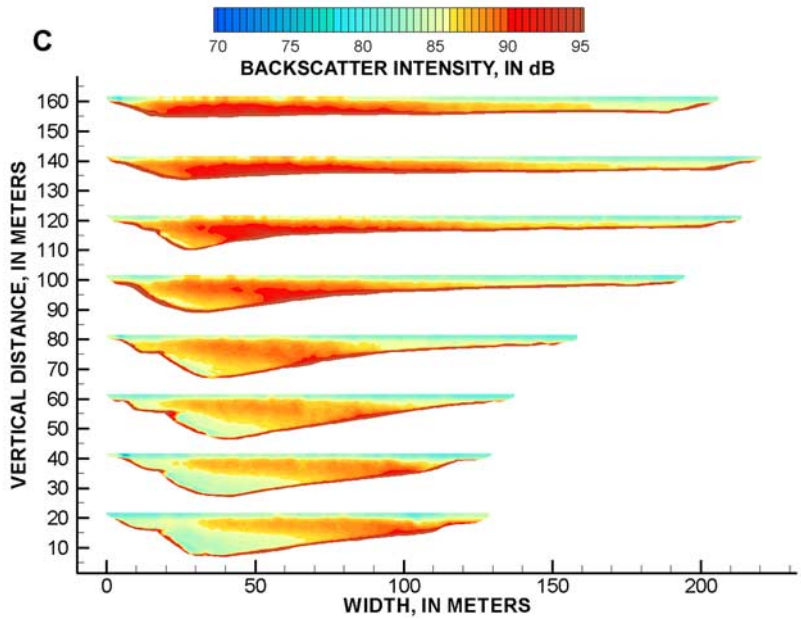

Figure 8. (continued)

velocities decrease. Although possibly recognized by some investigators, the radial fronts and incurvatures would not be detectable using depth-integrated suspended sediment sampling, and the cross-sectional outline of these structures was only discernible with the high resolution attained by the ADCP.

4.2. Aligning Cross-Stream Velocity Fields to Suspension Indicators

[48] Secondary circulation has been resolved in bend-crossing planes using a variety of methods, such as calculating residual vectors around the mean vector direction at measurement locations along the crossing line [*Rozovskii*, 1957; *Bathurst et al.*, 1977]. However, the cross-stream velocity field is not necessarily perpendicular to the mean vector directions at measured locations. The difference between derivations of secondary circulation and the cross-stream velocity field was discussed by *Dietrich and Smith* [1983]. To orient their cross-sectional velocity grids properly, they maintained streamwise continuity by matching cross-stream discharges (computed for various rotation angles) with predicted discharges. *Lapointe and Carson* [1986] alternatively defined the downstream velocity component (and thus the perpendicular crossing plane) by referring to the local cutbank trend at the water surface. More recently, studies of channel junctions with acoustic velocity measurements have noted similar ambiguities in defining secondary-circulation planes [*Lane et al.*, 2000].

[49] A boat path following the plane of the cross-stream velocity field could not be known before surveying. Instead, the survey boats followed radial sections that were drawn on a circle fitted to the entire bend. Averaged velocity grids for these routes happened to display the expected secondary circulation without additional adjustment. Inspection of the ADCP data showed that the outer margin of radial fronts corresponded with the extent of outward flow. Although turbulent advection/diffusion randomly altered the distribution of suspension indicators in single crossings (Figures 7a and 7b), the backscatter intensity of the averaged radial front decreased to background levels at the convergence zone over the outer bank pool. The flow-associated structure of the radial front and other suspension indicators suggested they could be exploited to refine a grid orientation representing the cross-stream velocity field.

[50] The cross-stream suspension indicators (Figure 8) evoked the dye tracer patterns inferred from studies of laboratory bends. *Fischer* [1969] measured dye concentrations in cross-stream traverses, one traverse near the surface and one near the bottom. He found the surface distributions were displaced toward the outside of the bend, and the bottom distributions toward the inside. More recently, *Boxall et al.* [2003] measured dye concentrations in cross-stream traverses using a vertical array of small sampling pipes. They concluded that the cross-sectional distribution of the dye plume depended on the injection point of dye. Along their laboratory bend, dye injected near the bed moved toward the inner bank, while dye injected near the water surface moved toward the outer bank. Laboratory observations also showed the secondary-flow influence on the central location of peak concentration within a dye plume [*Boxall et al.*, 2003; *Shiono and Feng*, 2003]. At the Clarksburg bend, a lateral region was identified near middepth where cross-stream velocities reversed direction. The highest backscatter intensities of the central channel were usually found in the same lateral region, again showing correspondence between the radial front and the dye tracer patterns in the laboratory.

[51] Supported by analogues in laboratory observations, we experimentally aligned cross-stream vectors to conform more closely with suspension indicators in backscatter planes. Exploratory rotations of the grid by only 2° to 3° altered the apparent pattern of secondary circulation in the velocity grid. To avoid ambiguity in the grid rotation, we

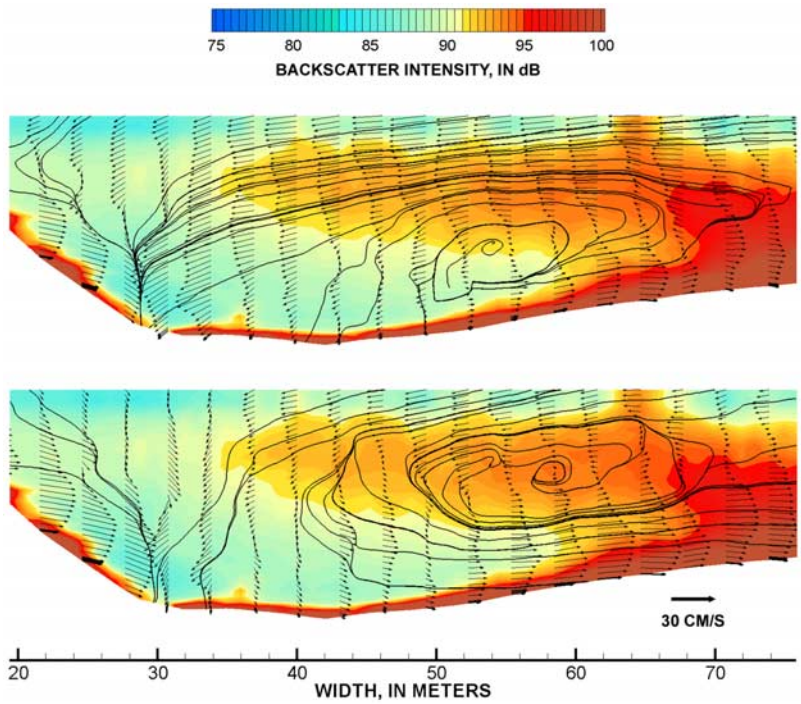

Figure 9. Cross-stream velocity vectors in averaged velocity grids at Clarksburg bend before and after reorientation to radial front (section 8, 14 March 2004). This example section was rotated 5°. Secondary circulation in each averaged velocity grid is represented by stream traces. Every third velocity ensemble is shown for clarity. Views are upstream.

hypothesized that minimal cross-stream velocity at the convergence zone explains the sudden lateral decrease in backscatter intensity. If true, the averaged velocity grid could be rotated to minimize cross-stream vectors approaching the convergence zone.

[52] This approach depends on the time-averaged Lagrangian response of suspended sediment distribution to the secondary flow. At each section, the averaged velocity grid contains an Eulerian measure of circulation, while the backscatter plane represents the integrated movement of suspended sediment achieved over some distance upstream from the crossing. From comparisons with symmetrical backscatter planes in straight reaches, one can infer that the outline of the asymmetric radial fronts represents cross-stream influences on advection of suspended sediment. Although the transport trajectory of suspended sediment does not follow the Eulerian circulation at any single section, the secondary-flow influence on the Lagrangian motion of particles is gradual and continuous through the bend. Therefore the direction of cross-stream velocity was compared with the apparent cross-stream influence on suspension indicators at all depths.

[53] The exploratory, interactive rotations were codified to reorient cross-stream velocity fields according to suspension indicators. First, the grids were rotated in the horizontal plane (with their interpolated vector components) to align with the x axis. The right bank of each grid was reset to the x-y origin. This set the elevation view of the grid to correspond with a rotation angle of zero. The grids were then rotated interactively in fractions of a degree around the z axis using Tecplot. Contours of backscatter intensity were given a repeating color map scale to highlight the steep gradients in suspension indicators. With minor rotations of the grid, the apparent directions of cross-stream components could be shifted left or right to match various suspension indicators.

[54] Three elements of the backscatter planes were used to guide the interactive alignment of averaged velocity grids: (1) aligning cross-stream convergence at the pool with steepest lateral gradient of the radial front, (2) dividing outward flow and inward flow along the center of the radial front to enclose the region of peak backscatter intensity, and (3) finding correspondence between inward flow and backscatter gradient within the incurvature. To find the optimum rotation, each grid was first rotated to display an apparent minimum of cross-stream vectors in the convergence zone. In response, the extent of outward flow immediately correlated with a steep lateral gradient of the radial front. Steep vertical gradients in the radial front near the pool also coincided with cross-stream flow along incurvatures. Each grid was then rotated by fractions of a degree to match cross-stream components of inward flow until mismatches occurred in other regions. Changes in cross-stream direction along vertical velocity profiles guided the rotation. Only a small range of rotation adjusted cross-stream velocity at middepth to a minimum within the peak backscatter intensity of the radial front. At greater rotation angles, the near-surface outward vectors would extend deeper down velocity profiles into the incurvature, or the inward vectors near the bed would extend higher into the outward advecting region of the radial front. Balancing the two tendencies in cross-stream flow forced a narrow determination of the final rotation angle, so that the amount of grid rotation was reproducible within 1° to 2° (Figure 9).

[55] After finding the optimum rotation, adjusted cross-stream and streamwise components u_n and u_s were derived by applying ϕ, the new angle of rotation from the x axis, in the transformation

$$u_n = u\cos\phi - v\sin\phi$$
$$u_s = u\sin\phi + v\cos\phi \quad (6)$$

where u and v are vectors originally referenced to x and y axes, respectively. This operation rotated the vectors with respect to the averaged velocity grid and displayed the cross-stream velocity field. At this stage, the cross-stream vector components were still contained in the 2-D grid matrix with a cross-sectional area based on the existing bathymetry. Depending on the revised orientation, the width of a section along the new angle would be wider or narrower by about 1%. For higher accuracy in cross-sectional properties, the ADCP crossings could be translated again along the reoriented section line to revise the averaged velocity grid.

4.3. Secondary Circulation in Reoriented Grids

[56] Secondary circulation in the cross-sectional plane was visualized with stream traces in Tecplot. The traces closely followed the Eulerian circulation in the crossing plane. Near the water surface, the negative bias in vertical velocity redirected stream traces unrealistically downward, which then followed the outward flow to the pool. Although the negative biases could not be corrected at ensembles in single ADCP crossings, mean offsets were applied across the negative bias zone in averaged velocity grids. Interior offsets were only 1 to 2 cm/s for the range of vertical velocity, which was on the order of ±12 cm/s.

[57] Stream trace origins were placed along the middepth of averaged velocity grids, with paths calculated in forward and reverse directions from the origins (Figure 9). With the optimum rotation applied, stream traces of secondary circulation became fully looped around the radial front (Figure 9b). A diagnosis and solution for errors in vertical velocity is still required before ADCP surveys can map cross-sectional secondary circulation reliably, without statistical corrections.

5. Discussion of Averaged Indicators of Secondary Flow

[58] The original motivation for ADCP surveys in bends was to assess the magnitude of cross-stream velocity for studies of salmon outmigrants in the Sacramento River. From the surveys at high discharge, we concluded that cross-stream velocities were indeed a significant fraction of streamwise velocity, often reaching 30 cm/s with mean streamwise velocities around 100 cm/s. This section describes the indicators of secondary flow at the Clarksburg bend from averaged velocity grids and backscatter planes. Although the intriguing results are presented with the most likely explanations, alternate hypotheses are considered here. Because the findings were derived solely from cross-sectional ADCP surveys, refutable tests of those findings are also suggested. Modified ADCP operations are proposed for similar studies in large rivers.

5.1. Secondary Flow in the Clarksburg Bend

[59] Plots of cross-stream velocity at sections 5 to 8 in surveys A–C are shown in Figure 10. After velocity grids were reoriented, the extent of inward flow near the bed was evident in adjacent sections. *Dietrich and Smith* [1983] concluded that, in the flow region over a point bar where cross-stream pressure gradient is exceeded by centrifugal force, no inward flow will be measured. They observed that inward flow was limited to 20 to 30% of the channel width, where flow depths were greatest. The adjusted cross-stream velocity fields of the Clarksburg bend were consistent with those findings, such that inward flows were confined to deeper portions of sections near the bend apex (Figure 10). Further downstream, the extent of inward flow across the point bar increased progressively, until inward flow approached the inner bank at the exit section.

[60] The outer bank at the Clarksburg bend had a submerged terrace about 7 m below the water surface, below which the bank was concave to the flow. The submerged terrace was about 5 m wide. The cross-stream flow above the terrace was directed toward the pool, but some velocity profiles above the terrace had shore-directed components. Along the lower, concave bank, cross-stream velocities were consistently directed toward the pool, with some being the highest magnitudes of the cross section (Figures 10a and 10b, sections 6 and 8). The cross-stream velocity of outward flow decreased in sections beyond section 5, while inward flow increased its extent up the point bar.

[61] Over the pool, near-surface outward flow converged with poolward flow from the outer bank, where negative vertical velocities were the highest in the cross section. In averaged velocity grids, positive vertical velocities were measured at the outer bank of section 6, with maximum values exceeding 3 cm/s. Less than 5 m away at the pool, river flow was dominated by strong downwelling at the pool, with minimal cross-stream velocity. Downwelling regions within the pool were measured consistently in the three surveys of the Clarksburg bend.

[62] The cross-stream velocity at each section maintained similar vertical distributions as discharge declined over the three surveys (Figure 10). To avoid subjective bias, the grid alignments for each survey episode were guided only by the suspension criteria, without reference to grids of other survey episodes. In all three surveys, near-surface outward flow decreased between sections 5 and 8, while inward flow reached its maximum extent toward the inner bank at section 8. Also, the highest cross-stream velocities for inward flow were measured near midchannel, where the maximum vector magnitudes in sections 5 to 8 declined from ~30 cm/s in survey A to ~15 cm/s in survey C. Average streamwise velocity declined from 110 to 58 cm/s over the same surveys (Table 1).

[63] Comparison of surveys A and B showed that bed elevation of the point bar rose by 1 to 2 m in less than a month. Although bed forms were not surveyed explicitly in this study, bed form heights were measurable from crossing bathymetry. In bathymetric grids at identical sections, bed form heights in both surveys A and B along the point bar had diminished to less than 0.1 m from those prevalent

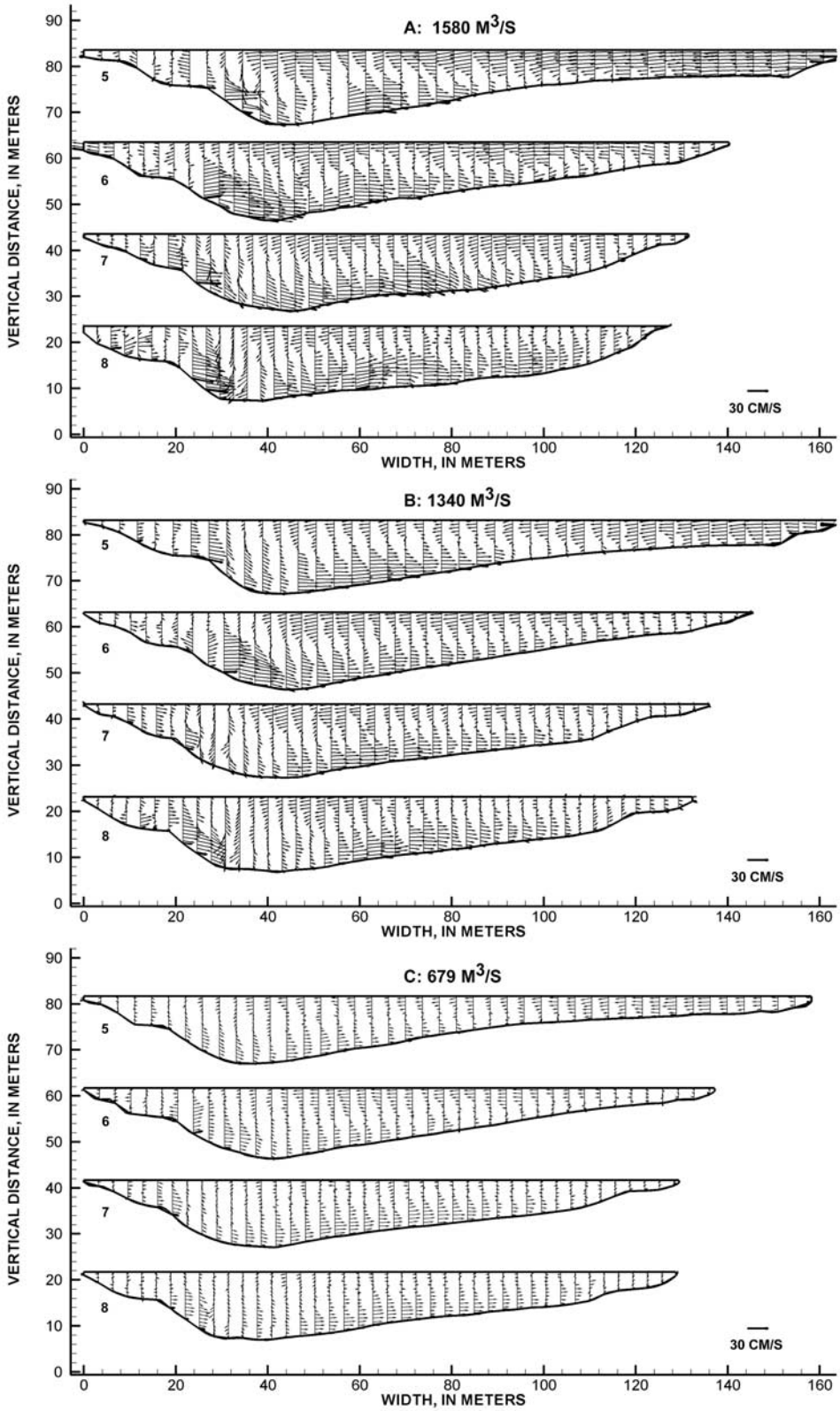

Figure 10. Cross-stream velocity vectors in averaged velocity grids for the Sacramento River at Clarksburg bend, surveys (a) A, (b) B, and (c) C, at sections 5–8. Velocity grids were reoriented to conform to suspension indicators as described in section 4 for averaged velocity grids. Every third velocity ensemble is shown for clarity. Views are upstream.

during reconnaissance surveys before peak discharge. The small bed forms at high discharge were consistent with a sequence of bed form diminishment and recovery previously documented in the lower Sacramento River [*Dinehart*, 2002].

5.2. Alternate Hypotheses for Radial Features

[64] Although the backscatter planes most likely indicate sediment suspension, the radial fronts and incurvatures in bends were not sampled for suspended sediment concentration. For this reason, the suspension indicators might be attributed to acoustic backscatter properties, rather than varying concentration. Two kinds of properties (acoustic range and particle size variations) are considered.

[65] 1. Are contour gradients in radial suspension indicators related to depth range and not concentration? By comparing backscatter planes at all sections of the bend, we observed the following. (1) Contour gradients in radial fronts were independent of flow depth and bed proximity. (2) Backscatter intensity within deep pools was about the same as shallow, near-bank regions of minimal cross-stream flow. (3) Incurvatures had a close correlation with cross-stream flow at the pool, and did not occur in similar depths away from the pool. (4) The backscatter intensity clouds found in straight, sand bed channels were not identified under incurvatures at the pool beds, suggesting that local sediment suspension is limited in the pool.

[66] 2. Might a change in particle size distribution produce the lower backscatter intensity regions defined as incurvatures? Analyses of backscatter intensity in fluvial environments indicate that the single-frequency response of ADCPs increases their uncertainty in predicting sediment concentration over a range of sediment diameters [*Gartner and Cheng*, 2001]. Because bed material measured in pools of bends is often coarser than the median grain diameter of the reach [*Parker and Andrews*, 1985], the change in backscatter intensity in the incurvature might be attributed to near-bed suspension of coarser sediment. However, this contradicts the finding by *Gartner* [2004] that greater particle sizes in suspended sediment increase the backscatter intensity measured by ADCP. If anything, an increase in backscatter intensity would be expected from an increase in scatterer size near the pool [*Lurton*, 2002, p. 81]. The simplest explanation we can offer for the incurvatures is that lower sediment concentrations produce lower backscatter intensity.

5.3. Testable Findings From ADCP Surveys

[67] Spatial sorting of bed material in meander bends has been analyzed as a bed load transport problem [*Parker and Andrews*, 1985; *Kawai and Julien*, 1996; *Julien and Anthony*, 2002] and as a process resulting from both bed load and suspended sediment transport [*Deigaard*, 1980]. We surmise that the incurvature associated with radial flow could indicate helical recirculation of suspended sediment to the inside point bar, and consequently influence spatial sorting of bed material. Although the finding was not anticipated during ADCP surveys, this hypothesis is testable by sediment concentration sampling near the pool of bends, especially at high discharge.

[68] The experimental procedure to align cross-stream velocity vectors by reference to backscatter planes requires physical confirmation because it depends partly on interpretive skill. Backscatter planes could provide ancillary data for resolving cross-stream components, which are critical to analyzing flow forces relevant to sediment transport [*Dietrich and Smith*, 1983]. The experimental procedure would be testable by measuring more closely the correspondence between radial flow and cross-stream suspended sediment transport. Such a test would find whether minimal cross-stream velocity coincides with the gradient boundary of the radial front in a Lagrangian reference frame. At lower flows, suspended sediment distribution in the bend may spatially lag the secondary flow as cross-stream velocity becomes weaker. The backscatter intensity still shows promise as a tracer for secondary-flow patterns, and should be investigated further.

5.4. Adapting ADCP Operations to Complex Flows

[69] At present, water resource agencies use ADCPs for discharge measurement at an increasing number of monitoring sites. As suggested previously, slightly modified ADCP operations can provide velocity data that are applicable in geomorphic research and numerical modeling. For instance, if standard discharge measurements followed linear cross-sectional paths, averaged velocity grids could be readily computed at a wide variety of channel configurations. Analysis of ADCP surveys in peak discharges showed that six crossings may be a practical minimum to approximate time mean velocity fields as described here (Appendix A).

[70] There are operational limitations to overcome in ADCP surveys. In highly unsteady or tidal flows, averages of multiple crossings will be biased, and other practical strategies are required to increase the number of velocity field measurements per unit time. Because of the ADCP design, the inner region of the velocity profile near the bed is usually unmeasurable [cf. *Kostaschuk et al.*, 2004]. Alternate measurements of shear velocity from ADCP velocity profiles would still permit calculation of the boundary shear-stress field from flow data. Shear velocity can be obtained from the turbulence statistics of stationary velocity profiles recorded by ADCPs over time [*Stacey et al.*, 1999]. Although cross-sectional ADCP surveys do not acquire such data, stationary velocity profiles are easily measured with ADCPs during the surveys.

[71] ADCP surveys can quickly measure cross-sectional velocity fields of meander bends that are much larger than commonly studied. On 30 March 2004, only seven hours of boat time were required for two hydrographers to obtain six crossings at each of eight sections, and to profile channel topography in a 1 km reach. Of course, multibeam sonar is more accurate and effective for bathymetry of large open channels, and the concentration correlations from multiple-frequency backscatter devices are less uncertain in varying particle sizes [*Thorne and Hanes*, 2002]. For many agencies, however, the cross-sectional resolution provided by repeated ADCP surveys alone could greatly exceed that obtained by older methods in large rivers.

6. Summary

[72] Averaging of ADCP surveys in a large, sand-bedded river produced 3-D velocity measurements with high resolution of secondary flow. Cross-stream velocity directions were apparently correlated with lateral features of backscat-

Table A1. Statistics for Averages of Interior Segments at Two Straight Reaches Shown in Figure 1[a]

Reach	Vector Component	Velocity in Averaged Segment, cm/s	Mean Standard Deviation of All Segments	Standard Deviation in Averaged Segment
Freeport[b]	streamwise	125	22.7	14.9
Freeport[b]	cross stream	6.2	18.2	6.6
Freeport[b]	vertical	−1.2	5.7	2.0
Walnut Grove[c]	streamwise	128	19.4	15.3
Walnut Grove[c]	cross stream	4.4	12.8	5.4
Walnut Grove[c]	vertical	−1.5	3.4	1.6

[a]"Averaged segment" represents mean of vector components from all interpolated velocity fields on a final, identical grid. See Figure A1 for graphs of standard deviations in intermediate segment averages.
[b]Ten segments.
[c]Six segments.

ter distributions near the pool of a meander bend. Cross-sectional velocity grids and interpolated backscatter planes were used to indicate cross-stream velocity fields and suspended sediment distributions. Determination of the cross-stream velocity profiles consequently resolved the streamwise velocity profiles for hydraulic analysis. Downstream changes in suspended-sediment distribution, cross-stream velocity, and secondary circulation were inferred from the series of bend surveys. By resurveying the Sacramento River near Clarksburg twice after peak discharge, flow field changes related to discharge variation were identified, and the generality of the procedure was verified. Numerical limitations of the averaged velocity grids were those of most ADCP measurements in large rivers, namely inadequate near-bed velocity measurement, and fluctuations in measured velocity vectors induced by brief sampling of turbulent velocity profiles.

[73] We devised methods to accommodate irregular boat paths at cross sections, and corrected navigational, bathymetric, velocity, and backscatter components of ADCP data. Backscatter planes of single ADCP crossings showed cross-sectional sediment distributions in a near-instantaneous view. The averaged velocity grids indicated regions of high shear and potential erosion at outer banks by displaying flow deflection, high vertical and cross-stream velocities, and increased backscatter intensity. These types of measurements could be used to diagnose hydraulic conditions near levees during peak discharge.

[74] In contrast with careful, deliberate studies of small streams, secondary flows in a large river were surveyed rapidly during high discharges. Although ADCP surveys cannot resolve velocity fields near the bed, they are suited to navigable channels where finer measurements by other means are impractical. Under flow conditions far from ideal, ADCP surveys showed features of meander bends that merit closer investigation, such as the poolward flow at outer banks and the possible helical recirculation of suspended sediment to the inner point bar.

Appendix A

[75] To quantify the effects of averaging multiple ADCP crossings, velocity grids were extracted from ADCP discharge measurements made in February 2004 at two straight reaches of the Sacramento River (Table A1). The site at Freeport is located downstream from a bridge spanning a straight reach of the Sacramento River. Each ADCP crossing consisted of more than 300 velocity ensembles. Interior segments were extracted from 10 interpolated velocity fields, with resulting dimensions of 150 m × 6.4 m, or 214 × 17 vector nodes. The other site above Walnut Grove is in the middle of a straight reach longer than 2 km. Interior segments were extracted from six interpolated velocity grids, with resulting dimensions of 76 m × 6.8 m, or 219 × 18 vector nodes.

[76] The ADCP settings for velocity ensembles and bottom-tracking rate were identical to the settings used in bend surveys. The ADCP crossings were first interpolated to grids with the same procedures of bend surveys. A rectangular segment approximating the channel width and depth was extracted from the interior of each interpolated velocity field. These interior segments excluded the near-surface and near-bed bins to avoid bed fluctuations and ranges of unmeasured velocity.

[77] In sequential averaging of interior segments, the standard deviation decreases at a rate depending on the order in which segments are averaged. To remove the effect of ordering, all subsets (1 and 2; 1, 2, and 3; etc.) of interior segments were averaged to obtain standard deviations of those combinations. The total number of combinations C of segments to average was determined by

$$C[n,r] = \frac{P[n,r]}{r!} \tag{A1}$$

where n is the number of interior segments, r is the number in each subset, and the function P represents permutations.

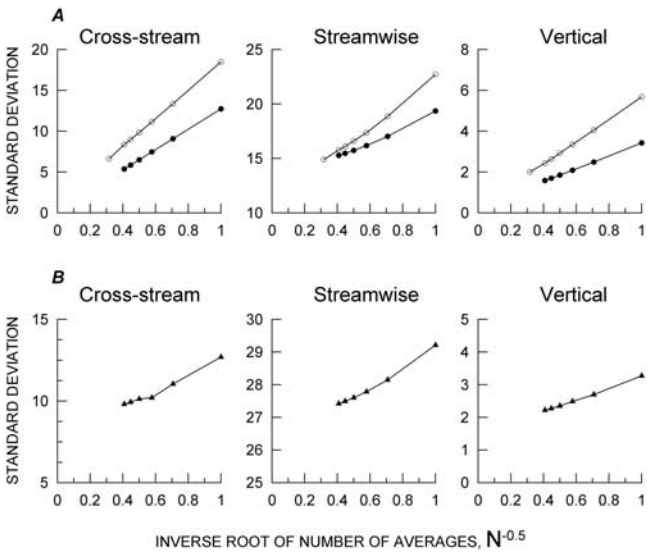

Figure A1. (a) Standard deviations for vector components of interior segments extracted from averaged velocity grids for Sacramento River at Freeport (open circles), measured during high discharge on 28 February 2004, and Sacramento River above Walnut Grove (solid circles), measured during high discharge on 29 February 2004. See crossing lines on Sacramento River (Figure 1) for location of measured reaches. (b) Standard deviations for vector components of central segment in averaged velocity grids at Clarksburg Bend, section 6, 14 March 2004.

All possible combinations C of segments r were averaged to obtain mean vector components and standard deviations for increasing n. Through this procedure, the measured decrease in standard deviation resulted only from an increasing number of averages, and not from fortuitous combinations.

[78] Standard deviations of spanwise and vertical components were reduced by half or more with more than five crossings (Table A1). Standard deviations of streamwise components were less reduced because they reflected vertical and lateral variations in velocity profiles across the channel segment. Averaged streamwise components retained a standard deviation near 15 cm/s. Decreases in standard deviations of cross-stream and vertical velocities were proportional to $1/N^{0.5}$, and trended toward zero at large N (Figure A1a). For cross-stream and vertical velocities in straight reaches, averages of multiple crossings approached zero with about six crossings. For the bend in Sacramento River near Clarksburg (Figure A1b), sequential averaging followed the $1/N^{0.5}$ proportionality. However, the standard deviation for spanwise components was offset from zero, due to vertical variation in secondary components from radial flow. The spanwise vectors reached a near-constant standard deviation with only three averages.

[79] **Acknowledgments.** Jon Yokomizo (USGS) obtained ADCP surveys in hazardous river conditions on several long days. James Best (University of Leeds) and Gary Wall (USGS) provided insightful discussion and prompted clarifications to a previous version. Comments by Daniel Parsons (University of Leeds) and two anonymous reviewers helped refine the presentation. The study was supported by projects of the CalFed Bay-Delta Authority, Sedimentation in the Delta, and Delta Cross-Channel Gate Operations. The use of trade, product, industry, or firm names in this report is for descriptive purposes only and does not constitute endorsement of products by the U.S. Government.

References

Ashworth, P., S. Bennett, J. Best, and S. McLelland (Eds.) (1996), *Coherent Flow Structures in Open Channels*, 733 pp., John Wiley, Hoboken, N. J.

Bathurst, J. C., C. R. Thorne, and R. D. Hey (1977), Direct measurements of secondary currents in river bends, *Nature*, *269*, 504–506.

Blanckaert, K., and W. H. Graf (2004), Momentum transport in sharp open-channel bends, *J. Hydraul. Eng.*, *130*, 186–198.

Boxall, J. B., I. Guymer, and A. Marion (2003), Transverse mixing in sinuous open channel flows, *J. Hydraul. Res.*, *41*, 153–165.

Bridge, J. S., and J. Jarvis (1982), The dynamics of a river bend: A study in flow and sedimentary processes, *Sedimentology*, *29*, 499–541.

Deigaard, R. (1980), Longitudinal and transverse sorting of grain sizes in alluvial rivers, *Ser. Pap. 26*, 108 pp., Tech. Univ. of Denmark, Lyngby.

Deines, K. L. (1999), Backscatter estimation using broadband acoustic Doppler current profilers, in *Proceedings of the IEEE Sixth Working Conference on Current Measurements, San Diego, CA, March 11–13, 1999*, pp. 249–253, IEEE Press, Piscataway, N. J.

Dietrich, W. E., and J. D. Smith (1983), Influence of the point bar on flow through curved channels, *Water Resour. Res.*, *19*, 1173–1192.

Dietrich, W. E., and J. D. Smith (1984), Bed load transport in a river meander, *Water Resour. Res.*, *20*, 1355–1380.

Dinehart, R. L. (1999), Correlative velocity fluctuations over a gravel river bed, *Water Resour. Res.*, *35*, 569–582.

Dinehart, R. L. (2002), Bedform movement recorded by sequential single-beam surveys in tidal rivers, *J. Hydrol.*, *258*, 25–39.

Dinehart, R. L. (2003), Spatial analysis of ADCP data in streams, paper presented at Sediment Monitoring Instruments and Analysis Research Workshop, Fed. Interagency Subcomm. on Sediment., Flagstaff, Ariz., 9–11 Sept.

Dinehart, R. L., and J. R. Burau (2005), Repeated surveys by acoustic Doppler current profiler for flow and sediment dynamics in a tidal river, *J. Hydrol.*, in press.

Fischer, H. B. (1969), The effects of bends on dispersion in streams, *Water Resour. Res.*, *5*, 496–506.

Gartner, J. W. (2002), Estimation of suspended solids concentrations based on acoustic backscatter intensity: Theoretical background, paper presented at Turbidity and Other Sediment Surrogates Workshop, Fed. Interagency Subcomm. on Sediment., Reno, Nev., 30 April to 2 May.

Gartner, J. W. (2004), Estimating suspended solids concentrations from backscatter intensity measured by acoustic Doppler current profiler in San Francisco Bay, California, *Mar. Geol.*, *211*, 169–187.

Gartner, J. W., and R. T. Cheng (2001), The promises and pitfalls of estimating total suspended solids based on backscatter intensity from acoustic Doppler current profilers, in *Proceedings of the Seventh Federal Interagency Sedimentation Conference*, vol. III, pp. 119–126, Fed. Interagency Subcomm. on Sediment., Washington, D. C.

Gordon, R. L. (1989), Acoustic measurement of river discharge, *J. Hydraul. Eng.*, *115*, 925–936.

Gordon, R. L. (1996), *Acoustic Doppler Current Profiler—Principles of Operation: A Practical Primer*, 2nd ed., 41 pp., RD Instruments, San Diego, Calif.

Grass, A. J., R. J. Stuart, and M. Mansour-Tehrani (1991), Vortical structures and coherent motion in turbulent flow over smooth and rough boundaries, *Philos. Trans. R. Soc. London, Ser. A*, *336*, 35–65.

Hill, D. C., S. E. Jones, and D. Prandle (2003), Derivation of sediment resuspension rates from acoustic backscatter time-series in tidal waters, *Cont. Shelf Res.*, *23*, 19–40.

Holdaway, G. P., P. D. Thorne, D. Flatt, S. E. Jones, and D. Prandle (1999), Comparison between ADCP and transmissometer measurements of suspended sediment concentration, *Cont. Shelf Res.*, *19*, 421–441.

Julien, P. Y., and D. J. Anthony (2002), Bed load motion and grain sorting in a meandering stream, *J. Hydraul. Res.*, *40*, 125–132.

Kawai, S., and P. Y. Julien (1996), Point bar deposits in narrow sharp bends, *J. Hydraul. Res.*, *34*, 205–218.

Kostaschuk, R. (2000), A field study of turbulence and sediment dynamics over subaqueous dunes with flow separation, *Sedimentology*, *47*, 519–531.

Kostaschuk, R., and M. Church (1993), Macroturbulence generated by dunes: Fraser River, Canada, *Sediment. Geol.*, *85*, 25–37.

Kostaschuk, R., P. Villard, and J. Best (2004), Measuring velocity and shear stress over dunes with acoustic Doppler profiler, *J. Hydraul. Eng.*, *130*, 932–936.

Land, J. M., and P. D. Jones (2001), Acoustic measurement of sediment flux in rivers and near-shore waters, in *Proceedings of the Seventh Federal Interagency Sedimentation Conference*, vol. III, pp. 127–134, Fed. Interagency Subcomm. on Sediment., Washington, D. C.

Lane, S. N., K. F. Bradbrook, K. S. Richards, P. M. Biron, and A. G. Roy (2000), Secondary circulation cells in river channel confluences: Measurement artefacts or coherent flow structures?, *Hydrol. Processes*, *14*, 2047–2071.

Lapointe, M. F. (1992), Burst-like sediment suspension events in a sand bed river, *Earth Surf. Processes Landforms*, *17*, 253–270.

Lapointe, M. F. (1996), Frequency spectra and intermittency of the turbulent suspension process in a sand-bed river, *Sedimentology*, *43*, 439–449.

Lapointe, M. F., and M. A. Carson (1986), Migration patterns of an asymmetric meandering river: The Rouge River, Quebec, *Water Resour. Res.*, *22*, 731–743.

Lurton, X. (2002), *An Introduction to Underwater Acoustics: Principles and Applications*, 347 pp., Springer, New York.

Nelson, J. M., and J. D. Smith (1989), Flow in meandering channels with natural topography, in *River Meandering*, *Water Resour. Monogr. Ser.*, vol. 12, edited by S. Ikeda and G. Parker, pp. 69–102, AGU, Washington, D. C.

Nezu, I., and H. Nakagawa (1993), *Turbulence in Open-Channel Flows*, 281 pp., A. A. Balkema, Brookfield, Vt.

Nystrom, E. A., K. A. Oberg, and C. R. Rehmann (2002), Measurement of turbulence with acoustic Doppler current profilers: Sources of error and laboratory results, in *Hydraulic Measurements and Experimental Methods 2002*, *Proceedings of the Specialty Conference, July 28–August 1 (2002), Estes Park, Colorado* [CD-ROM], Am. Soc. of Civ. Eng., Reston, Va.

Odgaard, A. J. (1981), Transverse bed slope in alluvial channel bends, *J. Hydraul. Div. Am. Soc. Civ. Eng.*, *107*, 1677–1694.

Parker, G., and E. D. Andrews (1985), Sorting of bed load sediment by flow in meander bends, *Water Resour. Res.*, *21*, 1361–1373.

Prandtl, L. (1952), *Essentials of Fluid Dynamics*, 149 pp., Macmillan, New York.

Rodriguez, J. F., F. A. Bombardelli, M. H. Garcia, K. M. Frothingham, B. L. Rhoads, and J. D. Abad (2004), High-resolution numerical simulation of flow through a highly sinuous river reach, *Water Resour. Manage.*, *18*, 177–199.

Rood, K. M., and E. J. Hickin (1989), Suspended-sediment concentration and calibre in relation to surface-flow structure in Squamish River estuary, southwestern British Columbia, *Can. J. Earth Sci.*, *26*, 2172–2176.

Rozovskii, I. L. (1957), *Flow of Water in Bends of Open Channels* (in Russian), 233 pp., Acad. of Sci. of the Ukrainian SSR, Kiev. (English translation, Isr. Program for Sci. Transl., Jerusalem, 1961.)

Shields, F. D., S. S. Knight, S. Testa III, and C. M. Cooper (2003), Use of acoustic Doppler current profilers to describe velocity distribution at the reach scale, *J. Am. Water Resour. Assoc.*, *39*, 1397–1408.

Shiono, K., and T. Feng (2003), Turbulence measurements of dye concentration and effects of secondary flow on distribution in open channel flows, *J. Hydraul. Eng.*, *129*, 373–384.

Simpson, M. R. (2001), Discharge measurements using a broad-band acoustic Doppler current profiler, *U.S. Geol. Surv. Open File Rep.*, *01-01*. (Available at http://pubs.water.usgs.gov/ofr0101)

Simpson, M. R., and R. N. Oltmann (1993), Discharge-measurement system using an acoustic Doppler current profiler with application to large rivers and estuaries, *U.S. Geol. Surv. Water Supply Pap.*, *2395*, 32 pp.

Stacey, M. T., S. G. Monismith, and J. R. Burau (1999), Measurement of Reynolds stress profiles in unstratified tidal flow, *J. Geophys. Res.*, *104*, 10,933–10,949.

Sumer, B. M., and R. Deigaard (1981), Particle motions near the bottom in turbulent flow in an open channel, part 2, *J. Fluid Mech.*, *109*, 311–337.

Thorne, P. D., and D. M. Hanes (2002), A review of acoustic measurement of small-scale sediment processes, *Cont. Shelf Res.*, *22*, 603–632.

U.S. Geological Survey (2001), Policy and technical guidance on discharge measurements using acoustic Doppler current profilers, *Tech. Memo. 2002.02*, Off. of Surf. Water, Reston, Va.

J. R. Burau and R. L. Dinehart, U.S. Geological Survey, 6000 J Street, Placer Hall, Sacramento, CA 95819, USA. (rldine@usgs.gov)